Topological Analysis of Experimental Electron Densities. 3. Potassium Hydrogen(+)−Tartrate at 15 K

T. Koritsanszky,[†] D. Zobel,[‡] and P. Luger*[,‡]

Department of Chemistry, University of the Witwatersrand, Private Bag 3, WITS 2050, Johannesburg, South Africa, and Institute for Crystallography, Free University of Berlin, Takustrasse 6, 14195 Berlin, Germany

Received: April 29, 1999; In Final Form: October 27, 1999

A charge density study of crystalline potassium hydrogen(+)−tartrate has been carried out using high-resolution X-ray diffraction data collected at 15 K. Three refinement models based on the rigid-pseudoatom formalism were tested to examine how the data resolution and restrictions on the anisotropic displacement parameters affect the topology of the static densities. The different experimental results and those obtained by Hartree−Fock calculations were compared in terms of bond topological properties of the densities. The Laplacian distribution, especially for the polar bonds, was found highly sensitive to the resolution of the data included in the fit and to the treatment of the displacement amplitudes. The restriction of these quantities, based on the ab initio intramolecular force field and invoked via rigid-bond (link) type constraints, turned out to be very efficient in controlling thermal deconvolution and reducing bias in the experimental density.

Introduction

The derivation of the static electron density ($\rho(\mathbf{r})$) of the crystalline state by X-ray diffraction measurements requires a detailed interpretation of the intensity data by means of an adequate model for the thermally averaged distribution of charge ($\langle\rho(\mathbf{r})\rangle$).[1] In the commonly used models[2,3] $\rho(\mathbf{r})$ is expressed in terms of nuclear-centered spherical harmonics augmented by Slater-type radial functions. This pseudoatomic static density is convoluted by the probability distribution function of the corresponding nuclear displacements to yield $\langle\rho(\mathbf{r})\rangle$. The model parameters are estimated by a least-squares (LSQ) fit of the observed reflection intensities or structure factor amplitudes. Inadequacies in the model or indeterminate variables cause bias in the parameter estimates. This problem is especially severe for noncentrosymmetric structures, such as the title compound, for which the procedure described above may lead to a physically meaningless result.[4] The inspection of the LSQ or the variance−covariance matrix can reveal hidden indeterminancies in the model in terms of linear dependencies or high correlation among variables. To furnish these mathematical relations with appropriate physical content is often a difficult or a hardly feasible practical approach. The usual practice is to try several models which differ in the selection of the variables. Applicable tests for the physical relevance of the mathematically equivalent LSQ solutions are limited.[5] It is thus desirable to introduce restrictions among the variables to support the physically most significant solution. A widely used approach to restrict the pseudoatom model is to apply chemical symmetry, i.e., to assume that equivalent atoms or functional groups having similar chemical environment must have the same contribution to $\rho(\mathbf{r})$. Another way to constrain the model is to impose local, noncrystallographic symmetry on the atomic density deformations. This can be achieved easily if the spherical harmonics are expressed in a properly chosen local coordinate systems attached to the atomic sites. In such local frames the symmetry restrictions on the pseudoatomic density can be formulated according to the index picking rules of the spherical harmonics corresponding to the assumed point group.[6]

A typical bias occurs in the anisotropic displacement parameters (ADPs) if $\rho(\mathbf{r})$ is based on a crude model such as the conventional, spherical-atom model. According to the test proposed by Hirshfeld[7] the bond-projected components of the displacement tensors (Z_A and Z_B) of a pair of bonded atoms (A and B) of comparable nuclear mass should not differ markedly ($\Delta_{AB} = Z_A - Z_B \approx 0$, where $Z_A = \bar{\mathbf{r}}_{AB}\mathbf{U}_A\mathbf{r}_{AB}$, $Z_B = \bar{\mathbf{r}}_{BA}\mathbf{U}_B\mathbf{r}_{BA}$, $\mathbf{r}_{AB} = \mathbf{r}_A - \mathbf{r}_B$ and $\mathbf{U}_A$ is the mean-squares displacement amplitude tensor of atom A). A significant deviation from the rigid-bond criterion could mean that the ADPs are biased by unresolved or indeterminable density asphericities. The test is based on the fact that Z_A and Z_B are associated with high-frequency, low-amplitude intramolecular stretching modes, resulting in a low value of Δ_{AB} for atoms A and B, forming a covalent bond. (Note that $\Delta_{AB} = 0$ for the external modes in the rigid-body approximation.) Such a "vibrational rigidity" can be considered as a "local symmetry" in the ADPs of the corresponding atoms, a symmetry which is best seen in a local frame, that is, in terms of the bond components of the ADP tensors. It is thus feasible to assume that independent information on Δ_{AB} values applied as restrictions in the fit of structure factors is likely to support the physically most significant LSQ estimation of parameters related to static density asphericities. The incorporation of intramolecular ADPs, calculated from *ab initio* force fields, into the refinement has shown to be a successful approach in the treatment of X-ray data of 1,2,4-triazole,[8] D,L-aspartic acid,[9] and diisocyanomethane.[10]

In the course of this study we examine in more detail the extent to which "rigid-bond" and "rigid-link" type constraints can reduce bias in the static parameters determining the experimental $\rho(\mathbf{r})$. To elucidate the effect of the restrictions applied, the static densities, obtained at different data resolutions

* To whom correspondence should be addressed. E-mail: luger@chemie.fu-berlin.de.
[†] University of the Witwatersrand.
[‡] Free University of Berlin.

10.1021/jp991418q CCC: $19.00
Published on Web 01/28/2000

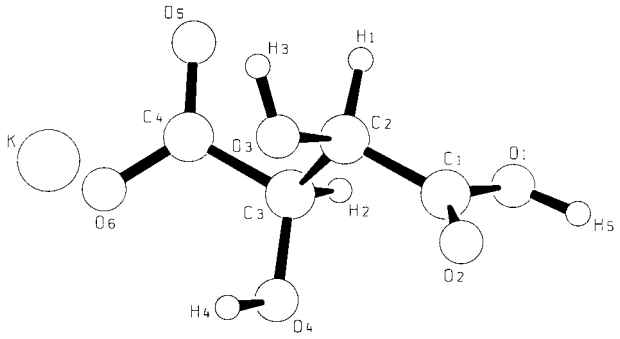

Figure 1. Molecular structure and atomic numbering.

and by different refinement models, are analyzed and compared in terms of their bond topological properties, such as the values of the $\rho(\mathbf{r})$ and its Laplacian ($\nabla^2\rho(\mathbf{r})$) at the bond critical points (CP) (at $\mathbf{r}_b$ where $\nabla\rho(\mathbf{r}_b) = 0$).[11]

The molecular and crystal structures of potassium hydrogen−tartrate (Figure 1) based on low-order data have been described earlier.[12] The anion has a wide variety of C−O bonds: alcoholic CC−OH and CO−OH type single bonds, double and delocalized double bonds in the COOH and COO^- groups, respectively. All but one oxygen atom are coordinated to the potassium cation, all three OH groups are donors, and the two oxygen atoms of the COO^- moiety are acceptors in hydrogen bonds.

Experimental Section

The crystal was mounted onto a beryllium needle sealed in a capillary (0.01 mm wall thickness) to prevent sublimation. The measurement was performed on a large four-circle Eulerian cradle (Huber, type 512) equipped with a double-stage closed-cycle He refrigerator (Air Products) and a Be vacuum chamber around the cold head. The vacuum was achieved with a turbomolecular pump up to less than 1×10^{-4} mbar and was stable during the entire measurement. The crystal was cooled to 15 K with a cooling rate of 1 K min^{-1}. During the cooling procedure several reflections were monitored by ϕ-scans to control the crystal quality. The alignment of the crystal was controlled by the C8 routine, based on centering of one reflection in eight equivalent positions.[13] Nb-filtered Mo Kα radiation was used at 50 KV and 40 mA (Seifert, ISO-Debyeflex 3000). The lattice parameters were obtained from 25 reflections with $11° < 2\theta < 32°$. Intensities were collected within a half-sphere in the range $0.05 < \sin(\theta)/\lambda < 1.09$ Å^{-1} in the bisecting mode. In the range $0.995 < \sin(\theta)/\lambda < 1.27$ Å^{-1} parallel mode data were also collected, but only a limited number of them were accessible owing to collision problems encountered with the large double-stage cryostat. This problem became even more severe with increasing 2θ, so that parallel mode data collection for $\sin(\theta)/\lambda > 1.09$ Å^{-1} was only attempted within a quarter sphere. The redundancy for the parallel mode data is thus lower than for that of the bisecting mode. No significant changes were observed in the intensities of the three standard reflections used. The merging of the symmetry-equivalent reflections (without Friedel pairs) collected in the bisecting mode led to an internal R value of 0.01. The data were corrected for Lorentz and polarization effects. An analytical absorption correction[14] was also applied, leading to minimum and maximum corrections of 1.002 and 1.004, respectively. Further experimental details can be found in Table 1.

Theoretical Calculations

Ab initio calculations were performed with the GAUSSIAN92 program package.[15] Full optimizations were carried out with the 6-311G** basis set at the Hartree−Fock (HF) and MP2 levels of theory starting from the X-ray structural data. As convergence criterion the threshold limits of 0.00045 and 0.0018 au were applied for the maximum force and displacement, respectively. The optimizations were followed by the evaluation of the harmonic vibrational frequencies (at the HF level) and internal vibrational amplitudes.[16] The topological analyses were performed on wave functions obtained from single-point calculations using the 6-311G** and $6-311^{++}$(3df,3pd) standard basis sets. These calculations were based on the experimental geometry (and optimized C−H and O−H distances) to allow for a direct comparison with the experimental density.

Density Models and Refinement Strategy

The generalized scattering factor expression applied is based on the Hansen−Coppens formalism[3] as implemented into XD, a computer package for refinement and analysis of experimental electron densities in crystals.[17] The quantity $\sum_{\mathbf{H}} w_{\mathbf{H}}(|F_{obs}(\mathbf{H})| - k|F_{calc}(\mathbf{H})|)^2$ was minimized using the statistical weight $w_{\mathbf{H}} = \sigma^{-2}(F_{obs}(\mathbf{H}))$ and only those structure factors which met the criteria of $F_{obs}(\mathbf{H}) > 3\sigma(F_{obs}(\mathbf{H}))$. The starting atomic parameters were taken from the earlier 100 K X-ray diffraction study.[12] The multipole expansion was truncated at the hexadecapolar level for the heavy atoms, while the deformation density of the hydrogen atoms was described by a bond-directed dipole. The core and the spherical valence densities were composed of HF wave functions expanded over Slater type basis functions.[18] For the deformation terms single-ζ orbitals with optimized Slater exponents were used.[18] The potassium cation was kept spherical (core-only scattering). No charge transfer between the cation and the anion was allowed, and the unit cell was kept neutral during the refinement. The two central carbon atoms, C(2) and C(3), were constrained to have the same valence deformation density. Similar restriction was applied to the hydrogen atoms in the O−H groups. The positional parameters of the hydrogen atoms were first refined against the data collected in the bisecting mode, and then the C−H and O−H distances were adjusted to 1.09 and 0.95 Å, respectively, by shifting the hydrogen atoms along the bond vectors obtained. These distances were maintained during subsequent refinements. The atomic numbering used is shown in Figure 1, while the definition of the atomic site coordinate systems can be found in Table 2. No local site symmetry was implemented. An isotropic extinction model of type 1 with Lorentzian distribution of mosaic spread[19] was also introduced. Different scale factors were refined for the bisecting and parallel mode data. The results presented in the next section are based on three models which differ only in the treatment of the displacement parameters.

In model 1 anisotropic and isotropic temperature parameters for the heavy and for the hydrogen atoms, respectively, were refined together with the positional and charge density parameters. This model corresponds to a conventional treatment and gives rise to 340 variables (341 − 1 due to the electroneutrality constraint): 104 core (99 positional and thermal parameters for non-hydrogen atoms and 5 isotropic displacement amplitudes for the hydrogen atoms) and 234 valence (229 multipole populations and 5 radial screening parameters), variables, in addition to the 2 scale factors and the extinction coefficient.

In model 2 the ADPs corresponding to internal vibrational modes generated from the ab initio (HF/6-311G**) harmonic force field were used as starting parameters. The displacement tensors, calculated in the inertial system, were first transformed into the local atomic frames on the basis of the optimized molecular geometry. The local frames were the same as those

TABLE 1: Crystallographic Data and Experimental Conditions

empirical formula	$K^+ (C_4H_5O_6)^-$	μ (cm^{-1})	8.27
cryst syst	orthorhombic	temp (K)	15(1)
space group	$P2_12_12_1$	scan type	$\omega-2\theta$
Z	4	step width $\Delta 2\theta$ (deg)	0.04
a (Å)	7.7355(8)	step width $\Delta\omega$ (deg)	0.02
b (Å)	10.5596(10)	scan width $\Delta\omega$ (deg)	$1.06 + 0.52 \tan \omega$
c (Å)	7.5959(9)	std reflns	(400), (006), (142)
V (Å^3)	620.40	data collectn range	
F(000)	384	bisecting mode 2θ (deg)	4−102
D_x (g/cm^3)	2.013	parallel mode 2θ (deg)	90−130
cryst size (mm^3)	0.30 × 0.32 × 0.31	hkl range	$\overline{19} \le h \le 19$, $\overline{14} \le k \le 22$, $\overline{16} \le l \le 17$
radiation	Mo Kα, Nb filter	N_{meas}	16909
λ (Å)	0.71069	N_{unique} (including Friedel pairs)	7482

TABLE 2: Definition of the Local Atomic Coordinate System[a]

atom	atom 0	AX1	atom 1	atom 2	AX2
O(1)	C(1)	X	O(1)	O(2)	Y
O(2)	C(1)	X	O(2)	O(1)	Y
O(3)	C(2)	X	O(3)	C(3)	Y
O(4)	C(3)	X	O(4)	C(4)	Y
O(5)	C(4)	Z	O(5)	O(6)	X
O(6)	C(4)	Z	O(6)	O(5)	X
C(1)	O(1)	Z	O(1)	O(2)	Y
C(2)	C(1)	Z	C(2)	C(3)	Y
C(3)	C(4)	Z	C(3)	C(2)	Y
C(4)	O(6)	Z	O(6)	O(5)	X
H(1)	C(2)	Z	C(2)	C(1)	X
H(2)	C(3)	Z	C(3)	C(2)	X
H(3)	O(3)	Z	O(3)	C(2)	Y
H(4)	O(4)	Z	O(4)	C(3)	Y
H(5)	O(1)	Z	O(1)	C(1)	Y

[a] The AX1, AX2 plane is defined by the atom 0−atom and atom 2−atom 1 vectors. The third axis is taken perpendicular to this plane, defining a right-handed system.

TABLE 3: Figures of Merit of Different Refinement Models[a]

	model 1	model 2	model 3
NVAR	340	295	318
$\sin(\theta)/\lambda$ [Å^{-1}]		1.27	
NREF		7348	
$R(F)$	0.0178	0.0191	0.0179
$R_w(F)$	0.0284	0.0294	0.0285
GOF	3.08	3.18	3.09
$\sin(\theta)/\lambda$ (Å^{-1})		1.09	
NREF		6462	
$R(F)$	0.0117	0.0135	0.0119
$R_w(F)$	0.0105	0.0122	0.0107
GOF	1.19	1.38	1.21
$\sin(\theta)/\lambda$ (Å^{-1})		0.85	
NREF		3162	
$R(F)$	0.0093	0.0103	0.0095
$R_w(F)$	0.0092	0.0102	0.0094
GOF	1.31	1.46	1.34

[a] NVAR, NREF ($|F| > 3\sigma(|F|)$), and GOF stand for the number of variables, number of reflections, and goodness of fit, respectively.

used for the spherical harmonics expansion. This was followed by transformations of the individual ADPs from their local frames to the crystal system. In this step the experimental molecular geometry was used. The procedure allows conformational differences between the calculated and observed structure to be accounted for. In each refinement cycle the shifts in the ADPs generated in such a way were restricted, via rigid-link type constraints, to fulfill the rigid-body motion requirement[20,21] ($6N - 20$ independent rigid-link constraints for a molecule comprised of N anisotropic atoms). For the hydrogen(+)−tartrate ion ($N = 15$, including the hydrogen atoms) the 70 linearly independent constraints, selected by the technique of singular value decomposition of the matrix of constraints, reduced the number of ADP components ($15 \times 6 = 90$) to 20 variables which are linear combinations of ADPs corresponding to the independent **T**, **L**, and **S** tensor components. The total number of variables was 295 ($16 \times 6 + 11 \times 3 = 129$ conventional parameters, 234 valence variables, and 2 scale factors reduced by 70 constraints on the ADPs and 1 on the monopole populations). We point out here that the approach applied allows one to assign ADPs even to the hydrogen atoms without refining all six individual components freely.

To account for the conformation differences between the optimized structure and that realized in the crystal, the constraints were restricted only to bonds and certain links between heavy atoms (model 3). During this refinement all links (bonds) in each of the following groups of atoms were considered to be rigid: [C(1),C(2),O(1),O(2),O(3)], [C(2), C(3),C(4)], [C(4),O(5),O(6)], and [C(3),O(4)], giving rise to 17 constraints. Since the ADPs of the hydrogen atoms were kept at the values obtained by refinement 2, the number of variables was reduced by 22 relative to that of model 1 ($340 - 17 - 5 = 318$). All three models were also tested against two limited data sets obtained with cutoff values of 1.09 and 0.85 Å^{-1} in $\sin(\theta)/\lambda$. The statistical figures of merit for the different refinements are given in Table 3. The multipole parameters based on model 3 are listed in Table 4.

Results and Discussion

The entries in Table 3 show that model 1 and model 3 led to almost the same fit with 340 and 318 variables, respectively. Model 2 appears to give the worst fit but with the highest reflections-to-variables ratio. The considerable increase in the weighted residuals due to the inclusion of the parallel-mode reflections suggests that for these data points the standard uncertainties were underestimated.

The differences in the structural parameters obtained by the different refinements lie within 3 times their standard uncertainties. In Table 5 some of the experimental (model 3) and optimized geometrical data are listed. There is a considerable departure from the expected symmetry in the experimental geometry of the COO^- group. The bond to O(6) is 0.0286 Å longer than that to O(5). This is not supported by either of the theoretical methods and could be attributed to the different crystal environments of these sites, since O(6) is involved in two hydrogen bonds while O(5) is involved in only one hydrogen bond. Similar distortion of the carboxylate group was found for the crystal structure of L-alanine,[22] D,L-aspartic acid,[9] and L-threonine.[23] The theory does not reproduce the experimental distances of the two equivalent C−OH bonds either. In the optimized molecule, in contrast to that found experimentally, the C(3)−O(4) bond is considerably longer than the C(2)−O(3) bond. The largest deviations between the optimized and

TABLE 4: Multipole Populations Based on Model 3[a]

	C(1)	C(2)	C(4)	O(1)	O(2)	O(3)	O(4)	O(5)	O(6)	H(1)	H(3)
κ	0.97	0.98	0.97	0.97	0.98	0.97	0.97	0.98	0.98	1.2	1.2
P_v	3.93	4.13	4.16	6.34	6.16	6.50	6.39	6.31	6.29	0.82	0.68
P_{11}	−0.10		0.04		−0.10	−0.08	−0.09	−0.10	−0.10		
P_{1-1}	0.11	0.04		−0.04		−0.09		−0.05			
P_{10}		0.12	0.06	0.06	−0.02		−0.06	0.04	−0.02	0.08	0.03
P_{20}	−0.24		−0.30	0.04		0.02		−0.07	−0.07		
P_{21}		−0.02		0.02		−0.02	0.07	0.04	0.03		
P_{2-1}		−0.08			0.05		−0.04	−0.02			
P_{22}	−0.04		−0.03	−0.06	−0.07	−0.11	−0.06	−0.08	−0.08		
P_{2-2}	−0.06	−0.04	−0.10	0.06	0.05		0.02		−0.04		
P_{30}			−0.06	0.03			0.04				
P_{31}	−0.05	−0.16			−0.02	−0.07	−0.07				
P_{3-1}	0.05	−0.19		−0.03	−0.02	−0.04	0.04				
P_{32}		−0.03	0.06		0.02	−0.05					
P_{3-2}		−0.05	0.04		0.02		−0.03				
P_{33}	0.32	0.16	0.32	0.09	0.04	0.05	0.03	0.02			
P_{3-3}	0.06	−0.08	0.05	−0.05		0.02			−0.02		
P_{40}					0.04	0.04					
P_{41}		−0.04				−0.05	−0.05				
P_{4-1}		−0.05					0.03	−0.05	−0.03		
P_{42}		−0.07		0.03	−0.03	−0.04	−0.03				
P_{4-2}			−0.10	−0.03	−0.03		−0.05				
P_{43}	0.05		−0.05								
P_{4-3}				0.06			0.06				
P_{44}		0.09			−0.02	0.04	0.05		0.04		
P_{4-4}		0.04					0.03		0.02		

[a] Only populations for which ($|P_{lm}| > \sigma(P_{lm})$) are listed.

TABLE 5: Selected Experimental and ab Initio Optimized Geometrical Parameters

bond	MP2/6-311G**	HF/6-311G**	exptl (model 3)
C(1)−C(2)	1.5072	1.5107	1.5201(8)
C(2)−C(3)	1.5403	1.5363	1.5381(8)
C(3)−C(4)	1.5598	1.5534	1.5341(8)
C(1)−O(1)	1.3743	1.3404	1.3172(9)
C(1)−O(2)	1.2159	1.1804	1.2196(9)
C(2)−O(3)	1.4123	1.3874	1.4193(9)
C(3)−O(4)	1.4214	1.3981	1.4093(8)
C(4)−O(5)	1.2674	1.2321	1.2450(8)
C(4)−O(6)	1.2624	1.2258	1.2736(8)

angles	MP2/6-311G**	HF/6-311G**	exptl (model 3)
C(1)−C(2)−C(3)	108.9	110.4	109.0(1)
C(2)−C(3)−C(4)	110.0	110.9	108.1(1)
O(1)−C(1)−C(2)	110.0	110.9	112.2(1)
O(2)−C(1)−C(2)	128.4	127.9	123.6(1)
O(3)−C(2)−C(3)	113.7	113.8	110.1(1)
O(4)−C(3)−C(2)	111.5	111.4	111.2(1)
O(5)−C(4)−C(3)	116.2	115.6	117.9(1)
O(6)−C(4)−C(3)	113.9	114.2	117.2(1)

dihedral angle	MP2/6-311G**	HF/6-311G**	exptl (model 3)
C(1)−C(2)−C(3)−C(4)	−204.0	−197.0	−179.8(1)
O(1)−C(1)−C(2)−C(3)	66.6	62.4	66.4(1)
O(2)−C(1)−C(2)−C(3)	−113.9	−119.6	−112.6(1)
O(3)−C(2)−C(3)−C(4)	35.0	40.5	57.5(1)
O(4)−C(3)−C(2)−C(1)	34.7	39.8	54.8(1)
O(5)−C(4)−C(3)−C(2)	37.1	34.4	54.5(1)
O(6)−C(4)−C(3)−C(2)	−142.1	−145.2	−123.2(1)

experimental molecular geometries occur in their relative conformations characterized by the dihedral angles at the C(2)−C(3) and C(3)−C(4) bonds. The carbon skeleton is found to be planar in the crystal, relative to which both optimized structures are distorted, which can be described by virtual rotations of about 20° around the central C(2)−C(3) and the C(3)−C(4) bonds. The optimized conformation seems to be stabilized via the O(6)···H(4) (1.951 Å) and the O(5)···H(3) (2.042 Å) intramolecular hydrogen bonds (the corresponding experimental values are 2.5199(6) and 3.0642(7) Å, respectively).

The differences in the projections of the intramolecular ADPs into the interatomic vectors (Δ_{AB}) are listed in Table 6, where the upper/lower triangular matrix refers to the optimized/experimental geometry. The comparison of the Δ_{AB} values generated for the crystal structure with those calculated for the optimized molecule reflects the conformational differences described above. For the C(2)···O(6), C(3)···O(2), O(1)···O(4), O(2)···O(4), and O(3)···O(6) links, the values deviate considerably. The complete set of rigid-link constraints based on the calculated ADPs and on the experimental conformation is thus not applicable. The inspection of the result obtained by the unconstrained refinement, on the other hand, indicates that the ADPs are biased by model 1. The Δ_{AB} values for the C−O bonds are 4−10 times larger than the theoretical ones. These observations suggest to limit the constraints to atom pairs of those segments which possess the same conformation in the crystal as in the optimized molecule. Thus, in model 3, only the (1,2) and (1,3) links mentioned before were considered.

The differences of the ADPs obtained by models 1 and 3 ($\Delta\mathbf{U} = \mathbf{U}_1 - \mathbf{U}_3$) can be visualized, by the computer graphics program PEANUT,[24] in terms of residual root-mean-square displacement surfaces at each atomic site. In Figure 2 the positive/negative lobes represent directions along which model 1 over/underestimates the atomic displacements with respect to model 3. The discrepancies are significant (except for O(5) and O(6)), but the pattern of the surfaces shows no features attributable to any specific vibrational mode.

The constraints on the ADPs manifest themselves also in changes in the multipole populations and thus in the total static $\rho(\mathbf{r})$. In Figure 3 a difference density map for the plane of the COO^- moiety is displayed which was obtained by subtracting the $\rho(\mathbf{r})$ of model 1 from that of model 3. This contour diagram shows, as is expected, features localized at the vicinity of the nuclei.

In view of the problem concerning model indeterminancies related to noncentrosymmetric stuctures, it is important to

TABLE 6: Difference Mean-Square Displacement Amplitude Matrix[a]

	C(1)	C(2)	C(3)	C(4)	O(1)	O(2)	O(3)	O(4)	O(5)	O(6)	H(1)	H(2)	H(3)	H(4)	H(5)
C(1)		1	0	1	0	−1	5	15	13	8	91	121	51	71	77
C(2)	0		−1	0	6	3	0	6	14	4	48	86	71	81	53
C(3)	−1	−1		0	21	12	4	0	3	2	90	48	130	72	92
C(4)	1	1	0		18	14	11	4	0	0	123	95	164	133	81
O(1)	0	6	21	18		−1	1	−10	0	−19	110	121	60	25	38
O(2)	0	4	17	14	−1		−2	−18	6	−8	88	110	35	68	124
O(3)	5	0	4	8	1	−2		0	9	5	74	67	40	137	66
O(4)	15	5	0	4	−5	−25	0		−2	3	64	75	138	40	164
O(5)	13	13	2	−1	−1	6	9	−3		0	124	102	92	133	41
O(6)	9	11	1	0	−18	−7	23	−2	0		116	94	168	113	114
H(1)	88	48	89	130	107	82	77	64	121	118		−2	15	−5	−64
H(2)	125	84	49	93	109	113	63	78	111	88	−2		52	17	−52
H(3)	84	68	94	182	90	84	20	63	155	174	1	23		−26	5
H(4)	188	131	65	151	115	213	141	13	134	213	47	−24	53		127
H(5)	72	51	71	56	36	121	64	116	37	68	−50	−48	−29	−35	

[a] The upper (lower) triangular matrix refers to the optimized (experimental) geometry. Units are angstroms. Entries are multiplied by 10^4.

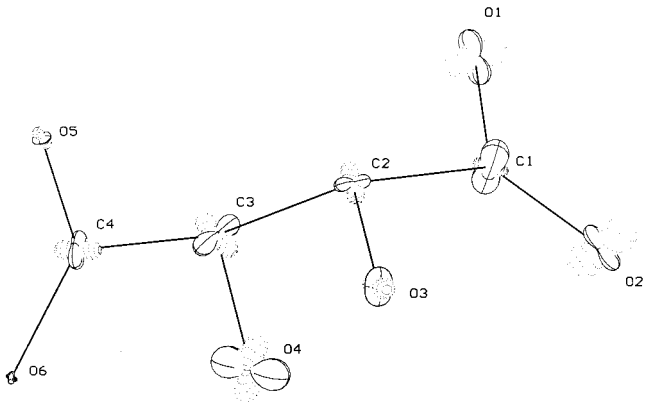

Figure 2. Residual root-mean-square displacement surfaces (positive/negative lobes drawn by solid/dotted lines) at each atomic site displayed with the computer graphics program PEANUT[24] (description in the text).

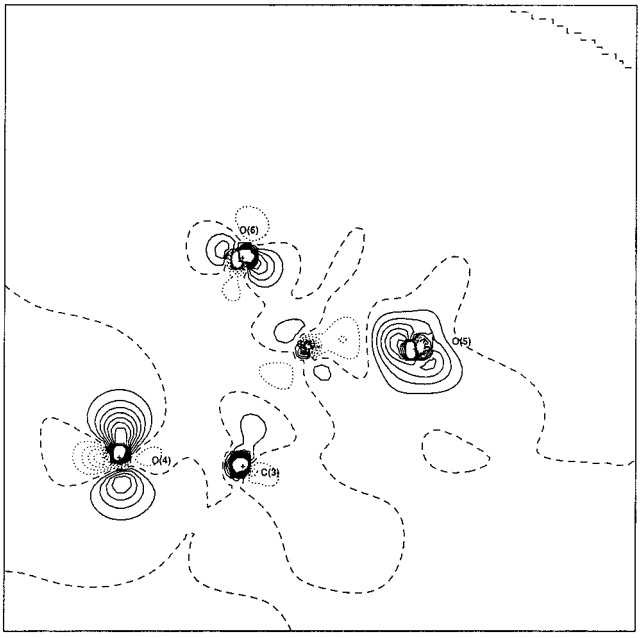

Figure 3. Difference between the electron densities obtained by model 1 and 3 in the plane of the carboxylate group (ρ(model 3) − ρ(model 1)). Contour intervals are 0.05 e/Å^3.

discuss the correlations between parameter estimates of the multipolar density. Large correlations (60−76%) found for both models are those between monopole populations and radial screening parameters. These correlations, which can amount to 80% even for centrosymmetric crystals, can be interpreted in a plausible way; that is, charge gain/loss must be accompanied by radial expansion/contraction of the valence shell. Other typical couplings, those which occur between ADPs and quadrupoles, are all below 70% for both models. Correlations between odd-order poles, being critical in the evaluation of the significance of a noncentrosymmetric density, are found to be less than 60%. Among the 30 correlation coefficients, all being below 70% for both models, 7 are associated with the coupling between positional parameters and dipole populations. From the analysis of the variance−covariance matrix, it can thus be concluded that no parameter estimates are severely ill-determined.

The topological analysis of the experimental $\rho(\mathbf{r})$ was performed using the property program XDPROP of the XD system,[17] while the theoretical density was interpreted with the program PROAIM.[25] Figures 4 and 5 show relief plots of the negative Laplacian function obtained from the wave function at the HF/6−311^{++}(3df,3pd) level and from the static density based on model 3. The Laplacian densities obtained by the two methods are very similar, though the bonded valence shell charge concentrations (VSCC) are more pronounced in the experimental than in the theoretical map. A quantitative comparison of the results of different refinements and theoretical calculations is given in Table 7 in terms of bond topological properties. The bond densities show relatively moderate model and basis set dependence. The $\rho(\mathbf{r}_b)$ values for the C−C and the C−O bonds agree within 10%. The trend in the strength of the covalent bonds revealed in this topological parameter is of chemical relevance. Both C−COO bonds are found to possess higher bond density than the C(2)−C(3) single bond. The C−O bond order decreases in the following order: C═OOH, C−OO$^-$, C−OHO, and C−OH. Considerable differences between theory and experiment are found for the $\nabla^2\rho(\mathbf{r}_b)$ values in the C−O bonds. Here the effect of introducing high angular momentum basis functions is especially pronounced. These findings are all in line with the results of a number of earlier studies on small organic molecules.[9,23,26−28]

Table 8 summarizes the changes in the topology of the experimental $\rho(\mathbf{r})$, obtained from models 1 and 3 for the carbonyl bonds, as a function of data resolution. For the unconstrained model (1) the bond CPs are found to be shifted toward the oxygen atoms as more high-order data are included. The shifts are accompanied by a decrease in the corresponding $\nabla^2\rho(\mathbf{r}_b)$ values for each bond. This trend is not reproduced by the constrained model, for which the topological indices considered show less sensitivity to the data extension. The effect

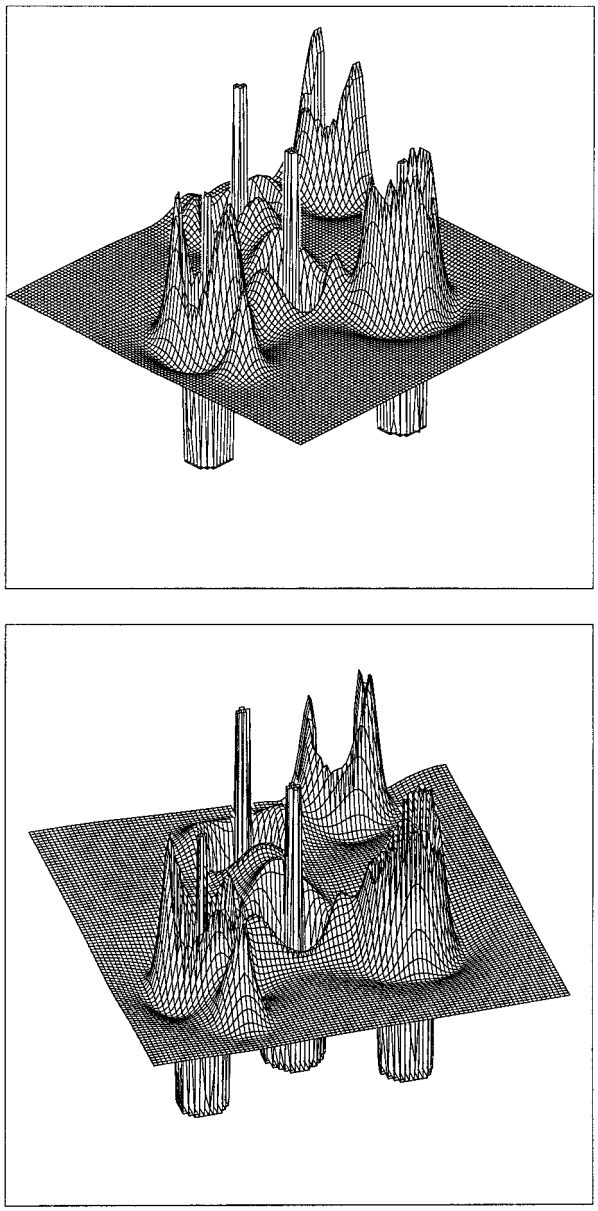

Figure 4. Experimental (top) and theoretical (bottom) negative Laplacian distributions in the C(1)−O(1)−O(2) plane. Orientation: O1−H left, C1 middle, O2 right.

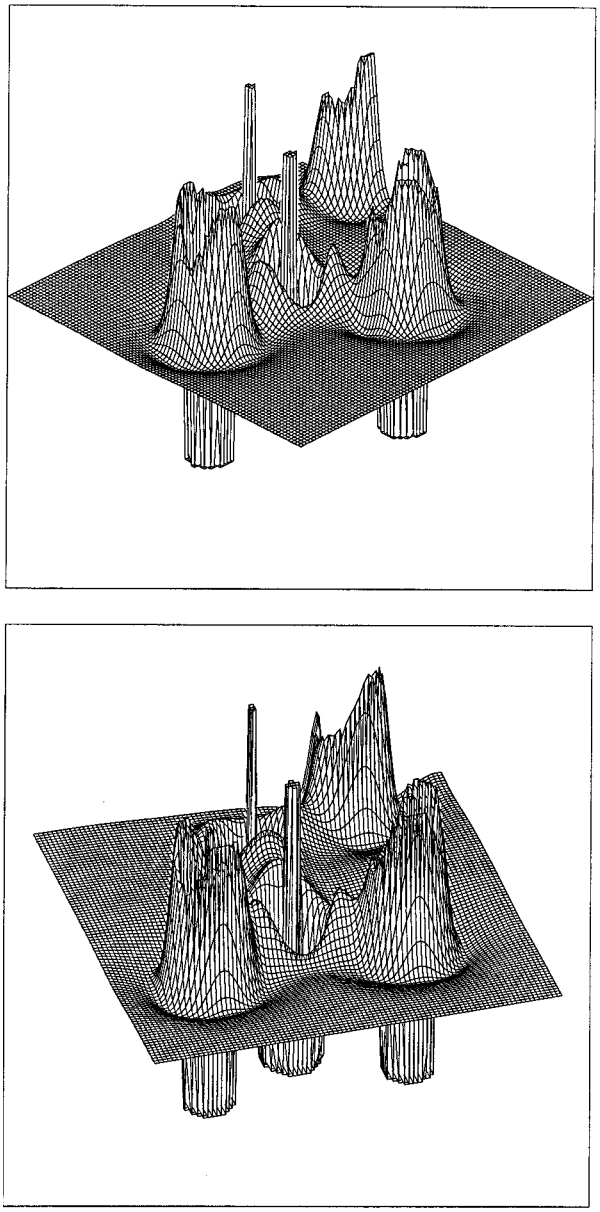

Figure 5. Experimental (top) and theoretical (bottom) negative Laplacian distributions in the O(5)−C(4)−O(6) plane. Orientation: O5 left, C4 middle, O6 right.

of inadequate deconvolution of thermal motion is demonstrated in more detail in Figure 6, where the negative Laplacian functions, obtained by different refinement models at different data resolutions, are plotted along the C(1)−O(2) bond path. Without the rigid-bond restriction (Figure 6a) the bonded VSCCs drastically change their location and size with decreasing number of high-angle data included in the refinement. This result is summarized in Table 9, where the values of the Laplacian functions at the (3,−3) CPs for the C(1)−O(2) bond are listed. As the result of limiting the data points used in refinement 1, the bonded VSCCs are shifted away from/toward the C(1)/O(2) nuclei. If only the low-order data are fitted, the bonded VSCC of the C(1)/O(2) atoms decreases/increases by around 100% compared to the values obtained by a full-data fit. These charge shifts are accompanied by considerable changes in the bond components of the ADPs of the C(1) and O(2) atoms ($\Delta_{AB} =$ 5, −1, and -7×10^{-4} Å^2 for high-, medium-, and low-order refinements, respectively). As is demonstrated in Figure 6b and by the corresponding entries in Table 9, the Laplacian is much less affected by the data resolution if the rigid-bond constraint is applied.

On the basis of this comparative analysis, model 3 can be considered as the most adequate of the three tested. The corresponding density was used to describe the strongest nonbonded interactions in the crystal. Table 10 contains the topological parameters for the O···H hydrogen bonds and the K^+···O contacts. Characteristic of closed shell interactions, the densities at the CPs are low with a slightly positive curvature. The CPs of the hydrogen bonds are located closer to the H atoms, while those of the K···O interactions are situated almost midway between the atoms.

Conclusion

From the analysis of the bond topological properties of the experimental electron densities obtained by different refinement models for potassium hydrogen(+)−tartrate, the following points emerged.

TABLE 7: Bond Topological Properties[a]

bond	model 1	model 3	HF/ 6-311G**	HF/ 6−311++G(3df,3pd)
C(1)−C(2)	1.74(6)	1.76(6)	1.83	1.80
	15.0(2)	15.3(2)	19.6	17.7
C(2)−C(3)	1.70(3)	1.69(3)	1.75	1.72
	11.6(1)	11.6(1)	17.1	15.7
C(3)−C(4)	1.80(6)	1.84(6)	1.80	1.77
	17.0(2)	17.6(2)	18.7	16.9
C(1)−O(2)	3.04(10)	2.91(10)	2.13	2.85
	45.6(7)	36.2(6)	1.0	17.8
C(4)−O(5)	2.75(10)	2.74(10)	2.61	2.76
	34.9(6)	34.8(6)	5.4	27.8
C(4)−O(6)	2.61(10)	2.65(10)	2.48	2.63
	36.9(6)	39.6(6)	10.4	30.3
C(1)−O(1)	2.22(10)	2.25(10)	2.77	2.21
	26.8(6)	28.5(6)	3.2	14.5
C(2)−O(3)	1.80(6)	1.81(6)	1.73	1.68
	15.6(3)	15.6(3)	6.4	8.1
C(3)−O(4)	1.84(3)	1.84(3)	1.75	1.68
	16.9(1)	16.7(1)	4.4	5.9
C(2)−H(1)	1.75(5)	1.78(5)	2.02	2.05
	15.9(3)	15.9(3)	27.2	28.7
C(3)−H(2)	1.80(5)	1.78(5)	2.00	2.05
	16.0(2)	16.0(2)	27.0	28.5
O(1)−H(5)	1.97(5)	2.00(5)	2.97	2.41
	20.5(2)	20.5(2)	61.1	69.6
O(3)−H(3)	2.08(5)	2.14(5)	2.38	2.42
	27.0(2)	28.2(2)	59.8	67.6
O(4)−H(4)	1.97(5)	2.03(5)	2.38	2.42
	22.7(2)	23.7(2)	60.4	68.4

[a] First row, the value of the charge density at the bond CP; second row, the negative Laplacian at the bond CP. For the comparison of the experimental Laplacians it is important to note that the standard uncertainties assigned to the $\nabla^2\rho(\mathbf{r}_b)$ values are underestimated in the present version of XDPROP, since the derivatives of this function with respect to the positional parameters and radial screening factors are ignored in the error calculation. Units are electrons and angstroms.

TABLE 8: Topological Properties of Carbonyl Bonds Based on Different Data Resolutions and Models[a]

bond/ resolution	model 1			model 3		
	$\rho(\mathbf{r}_b)$	$-\nabla^2\rho(\mathbf{r}_b)$	R(C−b)	$\rho(\mathbf{r}_b)$	$-\nabla^2\rho(\mathbf{r}_b)$	R(C−b)
C(1)−O(2)						
high	3.04(10)	45.6(7)	0.4551	2.91(4)	36.2(5)	0.4385
medium	2.91(9)	32.0(3)	0.4384	2.89(4)	32.3(5)	0.4424
low	2.84(10)	21.4(7)	0.4266	2.90(4)	31.7(5)	0.4396
C(4)−O(5)						
high	2.75(10)	34.9(6)	0.4750	2.74(4)	34.8(5)	0.4727
medium	2.78(9)	32.0(7)	0.4589	2.80(4)	33.3(5)	0.4663
low	2.72(10)	25.9(7)	0.4500	2.80(4)	32.8(5)	0.4698
C(4)−O(6)						
high	2.61(10)	36.9(7)	0.4550	2.65(4)	39.6(5)	0.4708
medium	2.51(10)	29.1(7)	0.4510	2.59(4)	34.6(5)	0.4676
low	2.39(10)	17.6(7)	0.4411	2.60(4)	34.8(5)	0.4796

[a] R(C−b) is the distance of the bond CP from the carbon atom. Units are electrons and angstroms.

The densities at the bond CPs, within the estimated experimental uncertainties, are in good agreement with the theoretical values, as well as with those obtained experimentally for chemically related compounds. This topological parameter, a useful indicator of the covalent bond strength, can indeed be reliably obtained from X-ray data.

The experimental Laplacian, although it exhibits all important features of atomic interaction in regions of key interest, its local topological characteristics are found to be sensitive to the choice of the model parameters and to the refinement conditions. The Laplacian based on the unconstrained refinement undergoes a considerable change in the polar bonds as the resolution of the data in the fit is increased. This is especially pronounced for

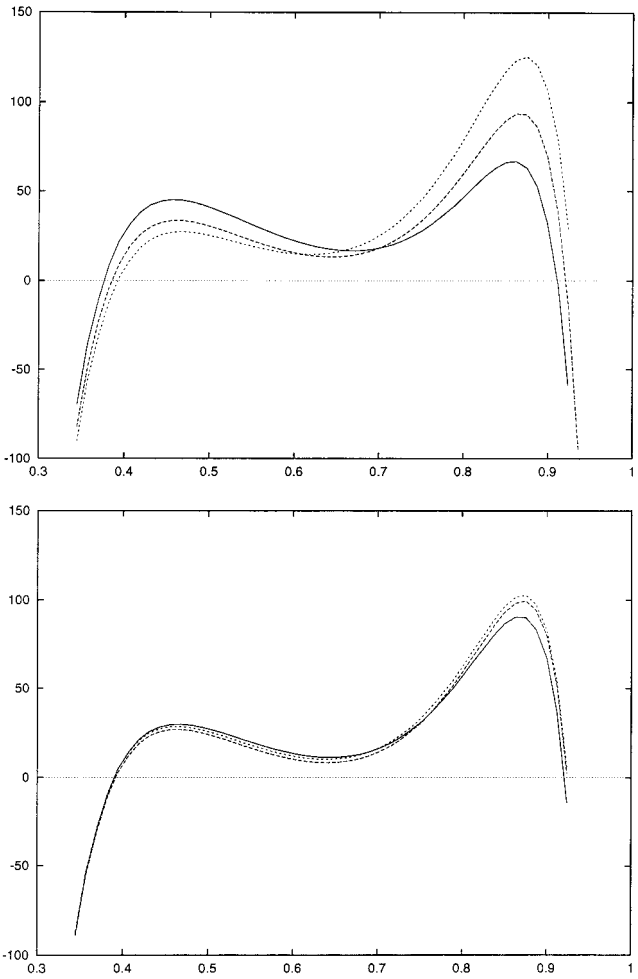

Figure 6. Experimental negative Laplacian functions (vertical axis in e/Å^5) along the C(1)−O(2) bond path (horizontal axis in angstroms) obtained by refinements against high (solid), medium (dashed), and low (dotted) order data: (a, top) model 1, lower (b, bottom) model 3.

TABLE 9: Topological Indices of the Bonded VSCCs of the Atoms in the C(1)−O(2) Bond[a]

atom/ resolution	model 1			model 3		
	$\rho(\mathbf{r}_c)$	$-\nabla^2\rho(\mathbf{r}_c)$	R	$\rho(\mathbf{r}_c)$	$-\nabla^2\rho(\mathbf{r}_c)$	R
C(1)						
high	3.03	45.8	0.4584	2.91	38.4	0.4628
medium	2.85	34.7	0.4622	2.83	34.2	0.4608
low	2.85	27.2	0.4671	2.91	33.3	0.4607
O(2)						
high	5.29	63.2	0.3600	5.55	95.7	0.3531
medium	5.75	95.4	0.3580	5.78	97.8	0.3499
low	6.23	128.7	0.3480	5.99	112.6	0.3487

[a] $\mathbf{r}_c$ is the location of the (3,−3) CP of the Laplacian, while R is the distance of the CP from the atom. Units are electrons and angstroms.

the C(1)−O(2) bond, which is becoming less polarized as seen in terms of an increase/decrease of the $\rho(\mathbf{r}_b)/\nabla^2\rho(\mathbf{r}_b)$ values and of an increase of the bonded VSCC of the C(1) atom at the expense of that of the O(2) atom. This tendency, found also for all polar bonds, is accompanied by significant changes in the ADPs which become less biased as more high-order data are included. Such an effect of the resolution on the parameter estimates is in line with the expectation and is a clear indication of pure thermal deconvolution owing to the lack of data and/or model inadequate, indeterminate variables. The rigid-bond constraint turns off the correlation between ADPs and static density parameters and leads to a topology of the polar bonds which is insensitive to the data resolution. The application of

TABLE 10: Geometrical and Bond-Topological Parameters for Closed Shell Interactions[a]

A···B	symm op/transl	R(A···B)	$\rho(\mathbf{r}_b)$	$\nabla^2\rho(\mathbf{r}_b)$	R(A−b)
O(6)···H(5)	x, y, z 0, 0, −1	1.5942(6)	0.44(3)	4.8(2)	1.0596
O(5)···H(4)	$1/2 + x, 1/2 - y, -z$ 0, 0, 0	1.8442(7)	0.23(3)	3.0(2)	1.1664
O(6)···H(3)	$1/2 + x$, 1/2 − y, $-z$ −1, 0, 0	1.8542(6)	0.22(3)	3.1(2)	1.1677
K^+···O(2)	$1/2 - x, -y, 1/2 + z$ 1, 1, −1	2.7032(7)	0.11(3)	2.1(2)	1.3891
K^+···O(2)	x, y, z 0, 0, −1	2.7529(6)	0.09(3)	1.7(2)	1.4249
K^+···O(4)	$1/2 + x, 1/2 - y, -z$ 0, 0, 0	2.7712(6)	0.09(3)	1.8(2)	1.4288
K^+···O(5)	$1/2 + x, 1/2 - y, -z$ −1, 0, 0	2.8571(6)	0.07(3)	1.4(2)	1.4691
K^+···O(5)	$-x, 1/2 + y, 1/2 - z$ 2, 0, −1	2.8794(7)	0.06(3)	1.3(2)	1.4844
K^+···O(3)	$1/2 - x, -y, 1/2 + z$ 1, 1, −1	2.9269(7)	0.06(3)	1.2(2)	1.5049

[a] R(A···B) and R(A−b) are the distances of atom A from atom B and from the corresponding bond CP, respectively. Units are electrons and angstroms.

this restriction seems to be of special importance for noncentrosymmetric structures and in the treatment of conventional data, i.e., those collected with the use of primary radiation generated by X-ray tubes.

The success of such applications depends primarily on the extent to which the molecular mean field approximation is applicable; i.e., how well can the intra- and intermolecular vibrational modes in crystals be separated? Another question is how the force field characteristic of the isolated molecule is to be modified to represent the intramolecular vibrational motion in the crystal. Due to crystal forces, the vibrational frequencies are expected to be shifted with respect to their values observed in the gas phase. Similarly, the thermal average of the nuclear configuration in the crystal can differ considerably from the equilibrium geometry of the isolated molecule. The first effect could be taken into account by scaling the diagonal elements of the calculated force constant matrix according to the frequencies observed in the crystalline state. The second problem needs a detailed analysis of the possibility to transform ADPs according to conformational differences between the ground-state, isolated molecular structure and the thermal-average nuclear configuration in the crystal. The procedure used in this study is correct to the extent to which local geometries are preserved during phase transition. In this respect (1,2) and (1,3) links play an inportant role, as the corresponding difference mean-square displacement amplitudes show a high degree of invariance with respect to changes in the chemical environment. The chemical transferability of these properties should be utilized, especially in the treatment of noncentrosymmetric structures. A data bank based on ab initio Δ_{AB} values is being built for such a purpose.

Acknowledgment. We thank the Deutsche Forschungsgemeinschaft (DFG) and the Fonds der Chemischen Industrie for financial support of this work. We are also grateful to the reviewers for their useful critical comments and suggestions.

Supporting Information Available: Tables of atomic coordinates and anisotropic displacement amplitudes obtained by both refinement models. This material is available free of charge via the Internet at http://pubs.acs.org.

References and Notes

(1) Stewart, R. F.; Feil, D. *Acta Crystallogr.* **1980**, *A36*, 503.
(2) Stewart, R. F. *J. Chem. Phys.* **1973**, *58*, 1668.
(3) Hansen, N. K.; Coppens, P. *Acta Crystallogr.* **1978**, *A34*, 909.
(4) El Haouzi, A.; Hansen, N. K.; Le Hénaff, C.; Protas, J. *Acta Crystallogr.* **1996**, *A52*, 291.
(5) Koritsanszky, T.; Buschmann, J.; Luger, P. *J. Phys. Chem.* **1996**, *100*, 10547.
(6) Kurki-Suonio, K. *Isr. J. Chem.* **1977**, *16*, 115.
(7) Hirshfeld, F. L. *Acta Crystallogr.* **1976**, *A32*, 239.
(8) Fuhrmann, P.; Koritsanszky, T.; Luger, P. *Z. Kristallogr.* **1997**, *212*, 213.
(9) Flaig, R.; Koritsanszky, T.; Zobel, D.; Luger, P. *J. Am. Chem. Soc.* **1998**, *120*, 2227.
(10) Koritsanszky, T.; Buschmann, J.; Lentz, D.; Luger, P.; Perpetuo, G.; Röttger, M. *Chem. Eur. J.* **1999**, *5*, 3413.
(11) Bader, R. F. W. *Atoms in Molecules—A Quantum Theory*; Clarendon Press: Oxford, 1990. See also: Souhasso, M.; Blessing, R. H. *Appl. Crystallogr.* **1999**, *32*, 210.
(12) Buschmann, J.; Luger, P. *Acta Crystallogr.* **1985**, *C41*, 206.
(13) King, H. G.; Finger, L. W. *J. Appl. Crystallogr.* **1979**, *12*, 374.
(14) Coppens, P.; Hamilton, W. C. *Acta Crystallogr.* **1970**, *A26*, 71.
(15) Frisch, M. J.; Trucks, G. W.; Schlegel, H. B.; Gill, P. M. W.; Johnson, B. G.; Wong, M. W.; Foresman, J. B.; Robb, M. A.; Head-Gordon, M.; Replogle, E. S.; Gomperts, R.; Andres, J. L.; Raghavachari, K.; Binkley, J. S.; Gonzalez, C.; Martin, R. L., Fox, D. J., Defrees, D. J., Baker, J., Stewart, J. J. P.; Pople, J. A. *Gaussian 92/DFT*, Revision G.1; Gaussian Inc.: Pittsburgh, PA, 1993.
(16) Higgs, P. W. *Acta Crystallogr.* **1955**, *8*, 99.
(17) Koritsanszky, T.; Howard, S.; Richter, T.; Su, Z.; Mallinson, P. R.; Hansen, N. K. *XD—a Computer Program Package for Multipole Refinement and Analysis of Electron Densities;* User Manual; Freie Universität Berlin: Berlin, 1995.
(18) Clementi, E.; Roetti, C. *Atomic Data Nucl. Data Tables* **1974**, *14*, 177.
(19) Becker, P. J.; Coppens. P. *Acta Crystallogr.* **1974**, *30*, 129.
(20) Schomaker, V.; Trueblood, K. N. *Acta Crystallogr.* **1968**, *B24*, 63.
(21) Didisheim, J.-J.; Schwarzenbach D. *Acta Crystallogr.* **1987**, *A43*, 226.
(22) Gatti, C.; Bianchi, R.; Destro, R.; Meratti, F. *J. Mol. Struct.: THEOCHEM* **1992**, *255*, 409.
(23) Koritsanszky, T.; Janczak, J.; Zobel, D.; Luger, P. Manuscript in preparation.
(24) Hummel, W.; Hauser, J.; Bürgi, H.-B. *J. Mol. Graphics* **1990**, *8*, 214.
(25) Cheeseman, J.; Keith, T. A.; Bader, R. F. W. *AIMPAC program package*; McMaster University: Hamilton, Ontario, 1992.
(26) Flensburg, C.; Larsen, S.; Stewart, R. F. *J. Phys. Chem.* **1995**, *99*, 10130.
(27) Koritsanszky, T.; Flaig, R.; Zobel, D.; Krane, H.-G.; Morgenroth, W.; Luger, P. *Science* **1998**, *279*, 356.
(28) Flaig, R.; Koritsanszky, T.; Janczak, J.; Luger, P.; Krane, H.-G.; Morgenroth, W. *Angew. Chem., Int. Ed. Engl.* **1999**, *38*, 1397.